Results of Examinations of Pressure Vessel Samples and Instrument Nozzles from the TMI-2 Lower Head*

by

G. E. Korth
Idaho National Engineering Laboratory
EG&G Idaho, Inc.
Idaho Falls, ID 83415

and

D. R. Diercks and L. A. Neimark
Energy Technology Division
Argonne National Laboratory
Argonne, IL 60439

October 1993

To be presented at the 21st Water Reactor Safety Meeting, Rockville, MD, October 25-27, 1993.

*Work supported by the Office of Nuclear Regulatory Research, U. S. Nuclear Regulatory Commission and by the Organisation for Economic Cooperation and Development.

Results of Examinations of Pressure Vessel Samples and Instrument Tube Nozzles from the TMI-2 Lower Head

G. E. Korth
Idaho National Engineering Laboratory

D. R. Diercks and L. A. Neimark
Argonne National Laboratory

Abstract

Fifteen prism-shaped steel samples were removed from the lower head of the damaged TMI-2 reactor pressure vessel to assess the effects of approximately 19 metric tons of molten core debris that had relocated there during the 1979 loss-of-coolant accident. Metallographic examinations of the samples revealed that inside surface temperatures of 800 to 1100°C were attained during the accident in an elliptical shaped "hot spot" ≈1 x 0.7 m. Tensile, creep, and Charpy V-notch specimens were also cut from the samples to assess the mechanical properties of the lower head material at temperatures up to the peak accident temperature. These properties were used in a margin to failure analysis of the lower head. Examinations of instrument nozzles removed from the lower head region assisted in defining the relocation scenario of the molten core debris and showed that the lower head was largely protected from catastrophic failure by a solidified layer around the molten core debris that acted as a partial thermal insulator.

Introduction

The TMI-2 Vessel Investigation Project (VIP) is an international program conducted jointly by the U.S. Nuclear Regulatory Commission (NRC) and the Organisation for Economic Co-operation and Development/Nuclear Energy Agency (OECD/NEA). The objectives of the program are to (1) determine a scenario for the Three Mile Island Unit 2 Nuclear Reactor loss-of-coolant accident in March 1979 and deduce the thermal history of the steel in the lower vessel head during the accident, (2) determine the mechanical properties of the lower head steel under the accident conditions, and (3) assess the integrity of the TMI-2 lower head under the accident conditions. Participants in the project include the U.S., Japan, Belgium, the Federal Republic of Germany (FRG), Finland, France, Italy, Spain, Sweden, Switzerland, and the United Kingdom (U.K.).[1-12]

The relocation of ≈19,000 kg of molten core debris onto the lower head of the reactor pressure vessel during the accident caused a considerable threat to the integrity of the pressure vessel. The lower head is comprised of 136-mm-thick A533B pressure-vessel steel with a 5-mm Type 308L stainless steel clad, and this quantity of molten debris had the potential of melting the lower head or causing it to fail by short-term creep under the tensile loadings present during the accident. The fact that the lower head did not fail indicates that significant melting did not occur and that time at temperature was not sufficient to produce creep failure under the loadings present. The purpose of the present investigation was to assess the extent of damage present in the lower head region, determine the maximum temperature of that material during the accident, and measure the mechanical properties of that material under the accident conditions.

Fifteen prism-shaped samples, each ≈152-178 mm (6-7 in.) long, 64-89 mm (2.5-3.5 in.) wide, and 64-76 mm (2-1/2-3 in.) deep, were recovered from the TMI-2 lower head during the first phase of the program (Fig. 1). The samples were cut from the inner surface of the lower head and typically extend through approximately half the lower head thickness. These 15 samples were subjected to detailed initial examinations and were then sectioned into metallographic and mechanical test specimens for further characterization (Fig. 2). The results of the initial sample examinations, metallographic studies, and mechanical tests are reported here.

In addition, 14 instrument nozzles and two guide tubes were removed from the lower head, and examinations of these components provided additional information on the core debris relocation scenario and the maximum temperatures attained during the accident. The results of these examinations are also reported here.

Initial Examination of Lower Head Samples

The 15 samples were received at Argonne National Laboratory (ANL) for visual examination, photography, dimensional measurement, and decontamination, to allow the subsequent machining operations to be relatively free of contamination.

The cladding surface of most samples was covered with a loose debris. Later analyses of scrapings of these surfaces indicated the material was principally an Fe-oxide with particulates of various core materials. A number of samples contained depressions of various shapes in the cladding, some of which appeared to be surrounded by locally melted cladding.

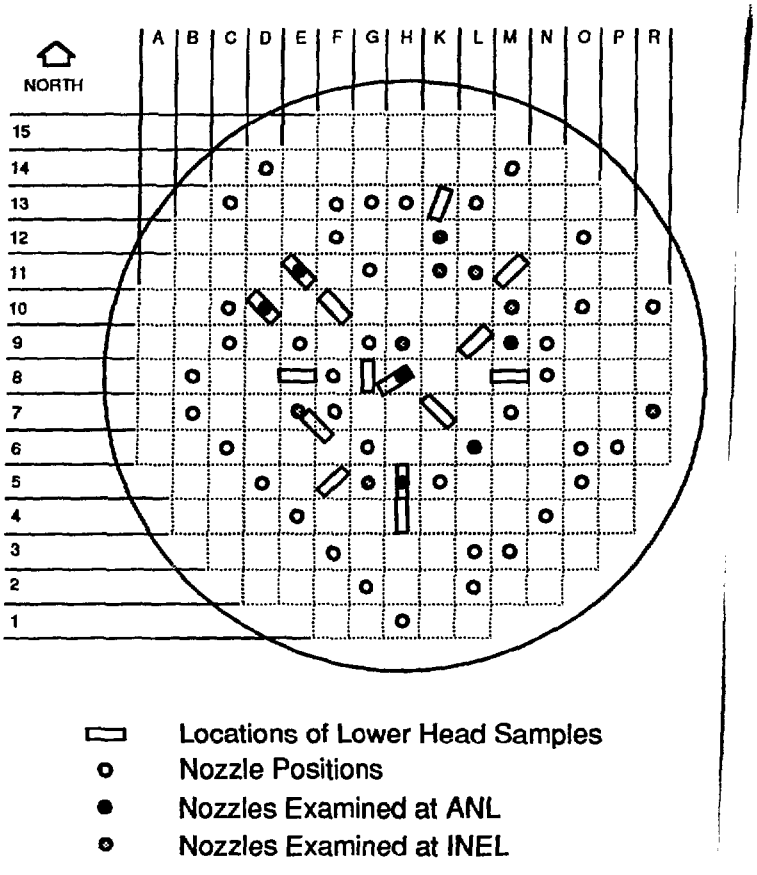

Fig. 1. Grid map of TMI core showing locations of lower head samples and nozzles.

Apparently these depressions were the result of false starts in the metal disintegration machining (MDM) method for removing the samples from the vessel. Also, the cladding at the end of the H-8 sample appeared to have separated from the vessel substrate. This was later attributed to the need to use mechanical force to pry this sample from the vessel.

The cladding on Sample E-6 was known to be cracked before its arrival at ANL. Cladding cracks were also seen at location G-6 in the lower head, but no sample was removed at this location. The visual inspection at ANL found the G-8 sample also be cracked, in a manner similar to that of E-6. Photographs of the cracks in E-6 and G-8 are shown in Fig. 3. These two samples were subsequently sectioned for metallographic and SEM-EDX analyses. Because of its cracks and the desire not to disturb the material within the cracks, sample G-8 was not chemically decontaminated as were the other samples. Its examination was done remotely in a hot-cell because of its high activity, whereas the other samples could be handled outside of a hot-cell after decontamination.

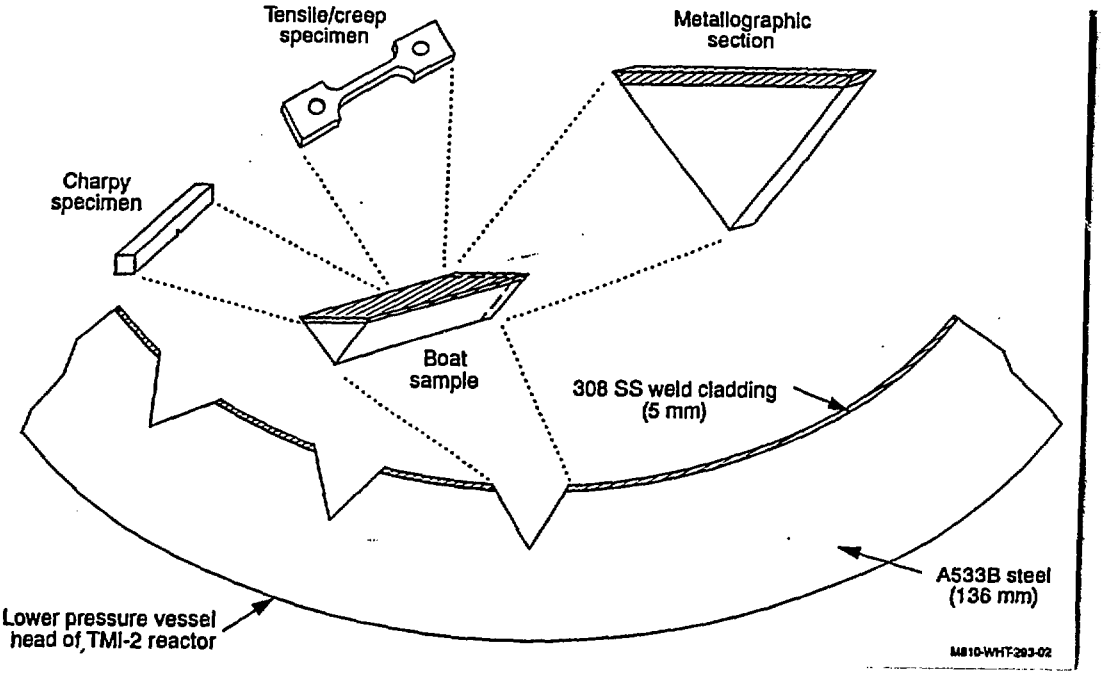

Fig. 2. Schematic of the source of the TMI-2 metallographic and mechanical property samples.

Sample decontamination was accomplished in a static bath of 50% solution of HCl in water for periods ranging from 50 min. to 5 hrs. For three samples it was necessary to use an additional 2-3 min. dip in concentrated nitric acid in order to get the samples down to acceptable activity levels. After these decontamination steps, it was possible to see the features of the original cladding weld passes on a number of samples. It was noted at that time that the cladding surface of sample F-10 contained micro-cracking at the grain boundaries in some of the weld passes. Because these micro-cracks have different morphology than the larger cracks in E-6 and G-8, they may or may not have resulted from the accident. The F-10 area, however, is on the edge of the hot-spot location found in the vessel.

Detailed Metallographic Studies

Following the initial examinations, metallographic specimens were cut from the lower head samples, decontaminated, and sent to the Idaho National Engineering Laboratory (INEL). These specimens were subjected to detailed characterization by optical metallography and hardness measurements to determine the maximum temperature attained at various lower head locations during the accident Supplemental examinations were also conducted by ANL and participating OECD partner laboratories.

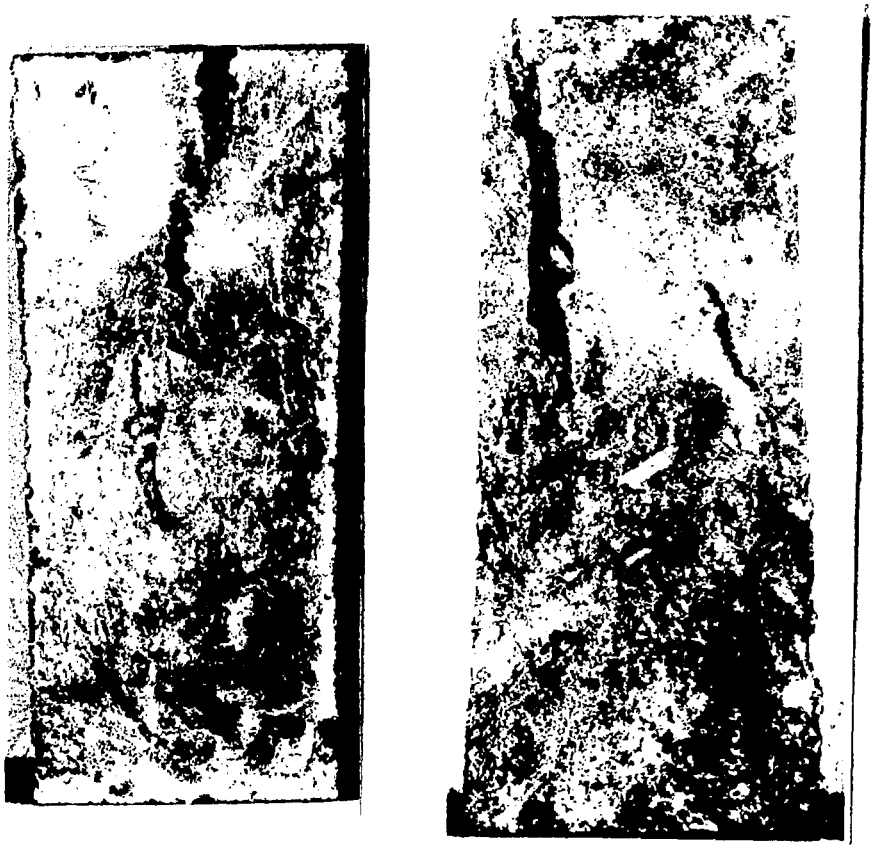

Sample E-6 Sample G-8

Fig. 3. Top views of Samples E-6 and G-8 showing cracking in the vessel cladding.

Background Information. The TMI-2 pressure-vessel lower head was fabricated from A533, Grade B low-alloy ferritic steel and clad for corrosion protection with Type 308L austenitic stainless steel using a multiple-wire submerged arc welding process. The fabrication history of the vessel is summarized as follows: 137 mm (minimum) plate formed to shape by hot pressing, austenitized at 871-899°C for 5.5 h, brine quenched and tempered at 649°C for 5.5 h, clad on the inside with 4.8 mm (minimum) ER308L stainless steel, and then stress relieved at 607°C for 50 h.

Since the amount of material extracted from the TMI-2 vessel was limited, archive A533B steel was also obtained from the abandoned Midland reactor, which had never been put into service. The Midland reactor pressure vessel was of the same vintage as the TMI-2 vessel, was built by the same contractor, and had a very similar fabrication history. The Midland

material was plentiful and provided a valuable resource for studying properties and accident-simulated thermal response of lower head material.

The weld cladding overlay and the fabrication history as described above left their "thermal signature" on the lower head. This as-fabricated condition was further thermally altered in some cases by the molten core debris that relocated during the accident. The typical as-fabricated condition (microstructure and hardness) as found in the TMI-2 and Midland lower head material is illustrated in Fig. 4. A heat-affected zone (HAZ) of 7 to 12 mm is observed in the A533B steel directly adjacent to the stainless steel weld clad. The first 2 to 3 mm of the HAZ is made up of enlarged, partially decarburized grains, and the remainder of this HAZ band is comprised of refined grains that reached temperatures above the ferrite-austenite transformation temperature of 727°C from the welding operation and were then quenched due to the massive heat sink provided by the remaining material thickness. Beyond the HAZ band, tempered bainite is observed uniformly throughout the remaining thickness. Any further thermal exposure equal to or greater than 727°C altered this as-fabricated structure and created a new thermal signature, which was used to determine the thermal history caused by the accident.

Three different methods of examination were used by the participating laboratories to assess the thermal history of the samples: (a) hardness profiles, (b) microstructure, and (3) thermally induced metallurgical modifications of the weld clad interface. The interfacial modifications were mainly a result of carbon diffusion from the A533B steel (≈0.25% C) into the 308L stainless steel clad (0.035% C max.). Typical hardness profiles were taken of the samples from the weld cladding to the bottom tip of the triangular piece. The microstructure was examined using standard optical metallographic practices. Electron microscopy (both scanning and transmission) were used by some laboratories in their examinations.

Hardness Measurements. The hardness profiles of most of the TMI-2 samples had the typical characteristic profile of as-fabricated material as shown in Fig. 4, but the hardness profiles from Samples E-6, E-8, F-10, and G-8 were markedly different than all other samples, as shown in Fig. 5. The characteristic hardness profile through the HAZ band had risen sharply in these four samples to much higher levels and was then sustained throughout the full sample depth. Heat-affected bands from the weld cladding were not evident in these four samples, but were completely eliminated by the thermal effects of the accident.

Two other samples (H-8 and F-5) also showed anomalies in the hardness profiles. Hardness measurements of H-8 in a longitudinal direction (parallel to the inside surface of the lower head) on several strips remaining after the tensile specimens were cut showed a hardness increase as the end closest to G-8 was approached. This observation indicates that the ferrite-austenite transformation temperature was reached on the end of H-8 nearest to G-8. The hardness profile of F-5, as measured by some of the participating laboratories, showed some deviation from the typical weld cladding HAZ effects, which indicates that temperatures in the vicinity of this sample slightly exceeded the 727°C threshold.

The final hardness of the TMI-2 samples is not only a strong indicator that the A533B steel transformation temperature of 727°C was exceeded during the accident, but also allows some bounds on the cooling rate back through the phase change. To achieve the same hardness values on standards as observed in Samples E-6, E-8, F-10, and G-8, the cooling rate had to be in the range of 10 to 100°C/min. Studies with the Midland material showed that if the cooling rate had been in the vicinity of 1°C/min or less, then the final hardness would have

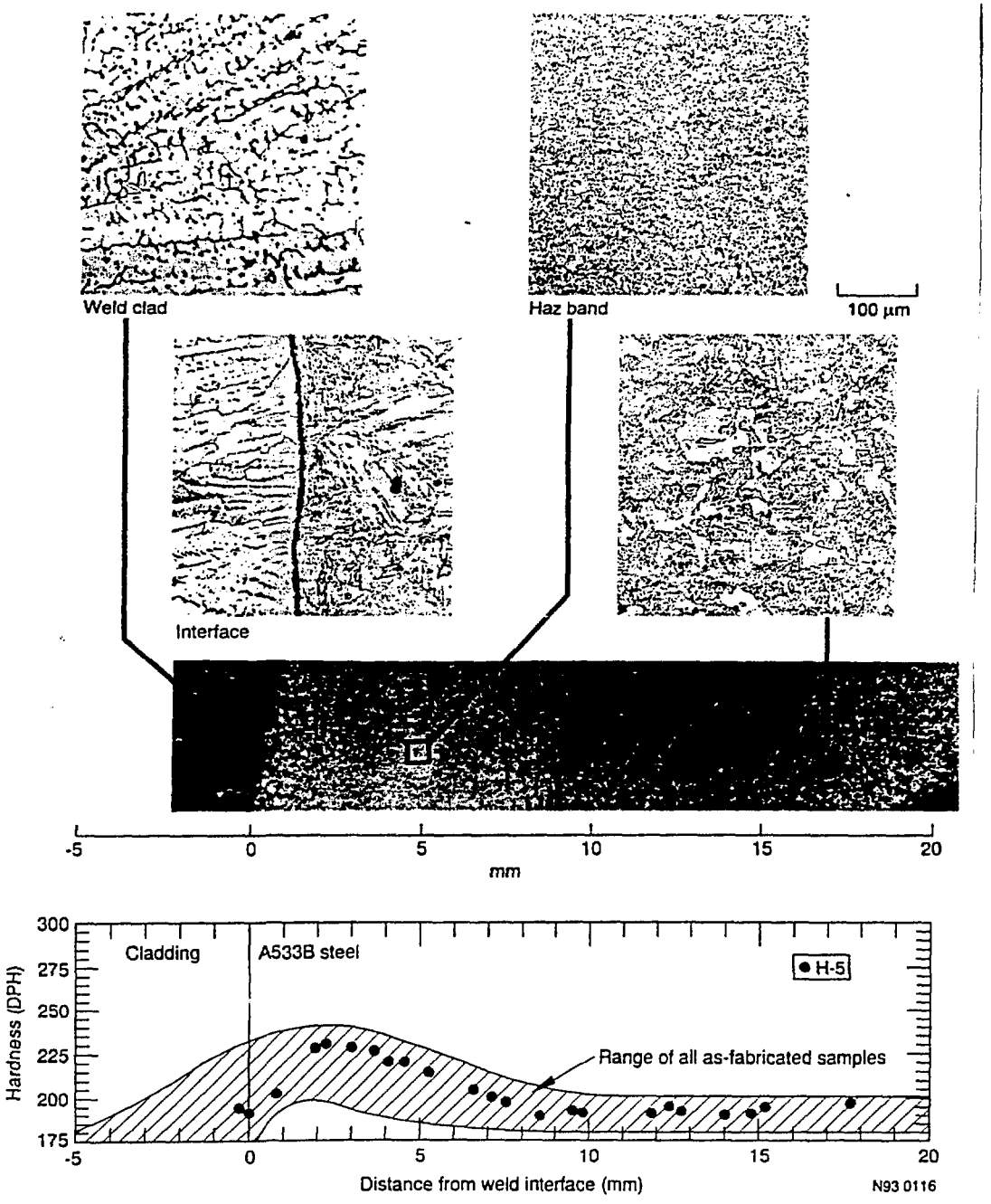

Fig. 4. Typical as-fabricated microstructure and hardness of TMI-2 lower head material (from Sample H-5).

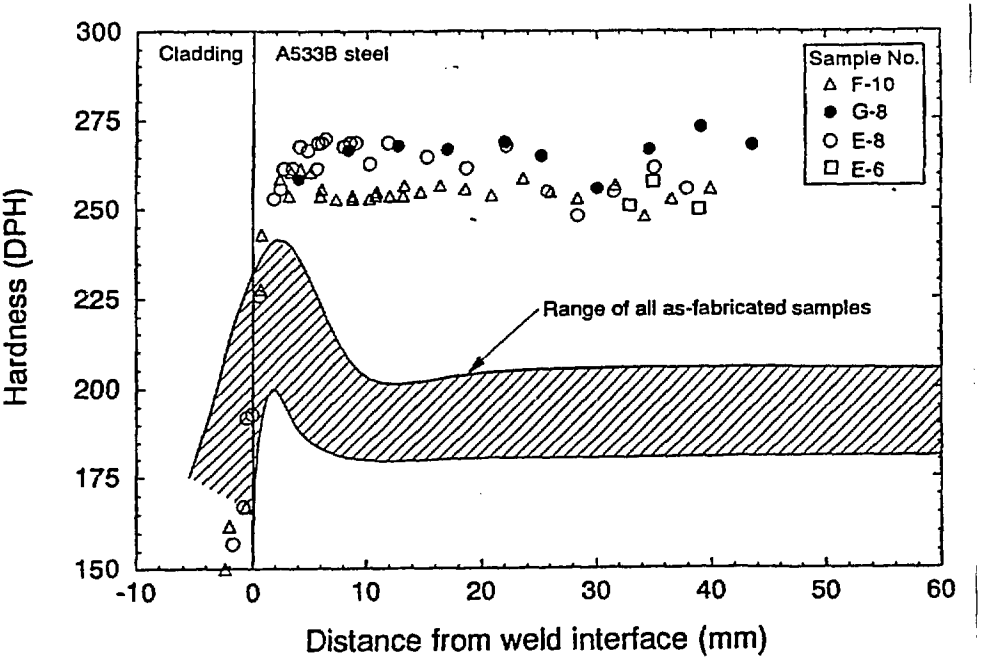

Fig. 5. Hardness profiles of Samples F-10, G-8, E-8 and E-6 compared to the as-fabricated samples.

been approximately the same as that of the as-fabricated parent metal. If that had been the case, hardness measurements would not have been very helpful in determining the thermal history due to the accident—they would only reveal that the hardness peak from the HAZ band from the weld cladding was eliminated. However, the final hardness values for E-8, F-10, G-8, and E-6 are consistent with cooling rates ≥10°C/min and any peak temperature above 800°C. Therefore, hardness values of the TMI-2 samples are indicative of two things: (a) whether or not the material had exceeded the transformation temperature, and (b) if it had, some bounds on the cooling rate. Hardness values are not very conclusive as to the peak temperatures that may have been reached even though some trends were observed by ANL and France. From just the hardness measurements, it was concluded that F-5 and one end of H-8 slightly exceeded 727°C and E-6, E-8, F-10, and G-8 exceeded 830°C. Examination of the microstructure was used to assess peak temperatures after the initial screening was performed with hardness measurements.

Midland Archive Standards. Standards with known thermal histories were prepared from Midland archive material and later from actual as-fabricated TMI-2 material. These accident-simulated standards provided a means for comparing a similar material with a known thermal history to TMI-2 material with an unknown thermal history. Initially, standards were prepared to determine the effect of cooling rate through the austenite-ferrite transition temperature range, which affects the hardness. Then, several laboratories prepared standards from Midland archive material with maximum temperatures that ranged from 700 to 1300°C

and with dwell times at peak temperatures of one minute to two hours. The heatup rate was controlled at 40°C/min, and the cooling rate following the dwell period was 1 to 100°C/min. Finally, as unknown thermal histories were narrowed down, an additional set of standards was prepared from some actual TMI-2 lower head material determined to be in the as-fabricated condition. These small sections of TMI-2 material were heat-treated at 950, 1000, 1050, and 1100°C for dwell times of 10, 30, and 100 minutes and provided the final basis for comparison to determine the thermal history of the lower head due to the accident.

As the standards were prepared and examined, various metallurgical observations revealed a step-wise process that could be used in determining the thermal histories of the TMI-2 samples. A diagram (shown in Fig. 6) was constructed, which illustrates the metallurgical changes with time and temperature of the Midland and TMI-2 lower head A533B steel with a 308L stainless weld clad. Since the vessel was stress relieved at 607°C after the weld cladding, no thermal effects from the accident could be detected at or below this temperature and, therefore, the diagram shows only metallurgical observations for temperatures above this point. The lowest temperature indicator, above the stress relief temperature, was the ferrite-austenite transformation, which starts at 727°C and is complete by ≈830°C. Variations in the typical as-fabricated hardness profile will be evident when this threshold is exceeded. The next indicator is the dissolution or dissipation of a dark feathery band at the interface; this occurs between 800 and 925°C, depending on the time. The next indicator of increasing temperature is the appearance of small equiaxed grains, which formed in the A533B steel adjacent to the interface at temperatures between 850 and 900°C and disappeared between 1025 and 1100°C as they were consumed by grain growth in the low alloy steel. The equiaxed grains, which are not typical for a low alloy steel, appear to be devoid of cementite, probably due to a loss of carbon into the stainless steel. Grain growth in the A533B steel becomes significant above approximately 950 to 1075°C, depending on the time involved. The highest temperature indicator shown on the diagram is the change in morphology of the δ-ferrite islands in the stainless steel cladding. In the approximate range of 975 to 1000°C at 100 minutes or 1100 to 1125°C at 10 minutes, the δ-ferrite islands begin to lose their slender branch-like morphology and become spherical in shape. This spheroidizing of the δ-ferrite islands is believed to be associated with the dissolution of $M_{23}C_6$ carbides, which decorate the ferrite-austenite boundaries and stabilize their shape. When the carbides dissolve, the δ-ferrite becomes more spherical to minimize surface energy. There was also evidence that some of the δ-ferrite was consumed into the austenitic matrix after exposures above 1000°C since there was a net loss of δ-ferrite after cooling. Researchers in the Federal Republic of Germany[7] and Spain[9] observed that δ-ferrite in the cladding of non-affected samples was 4-5%, but only 1.4% in E-8.

Microstructure of TMI-2 Samples. To further assess the thermal history of the four samples clearly showing thermal effects above the ferrite-austenite transformation temperature, microstructural indicators illustrated in Fig. 6 were employed. Examinations of the microstructure of E-6, E-8, F-10, and G-8 showed that the dark feathery band had dissipated at the A533B steel/weld cladding interface in all four samples. Austenitic grain growth was evident in all four samples, with E-6 and E-8 showing the most pronounced effect. F-10 revealed that a small remnant of the cementite-devoid equiaxed small ferrite grains were still present, but none was evident in the other three. Spheroidization of the δ-ferrite islands in the weld cladding was not readily detected in F-10, was partially observed in G-8, and was fairly significant in E-6 and E-8. By applying the above microstructural observations and meticulous comparisons with the standards of known thermal history, the lead laboratory for

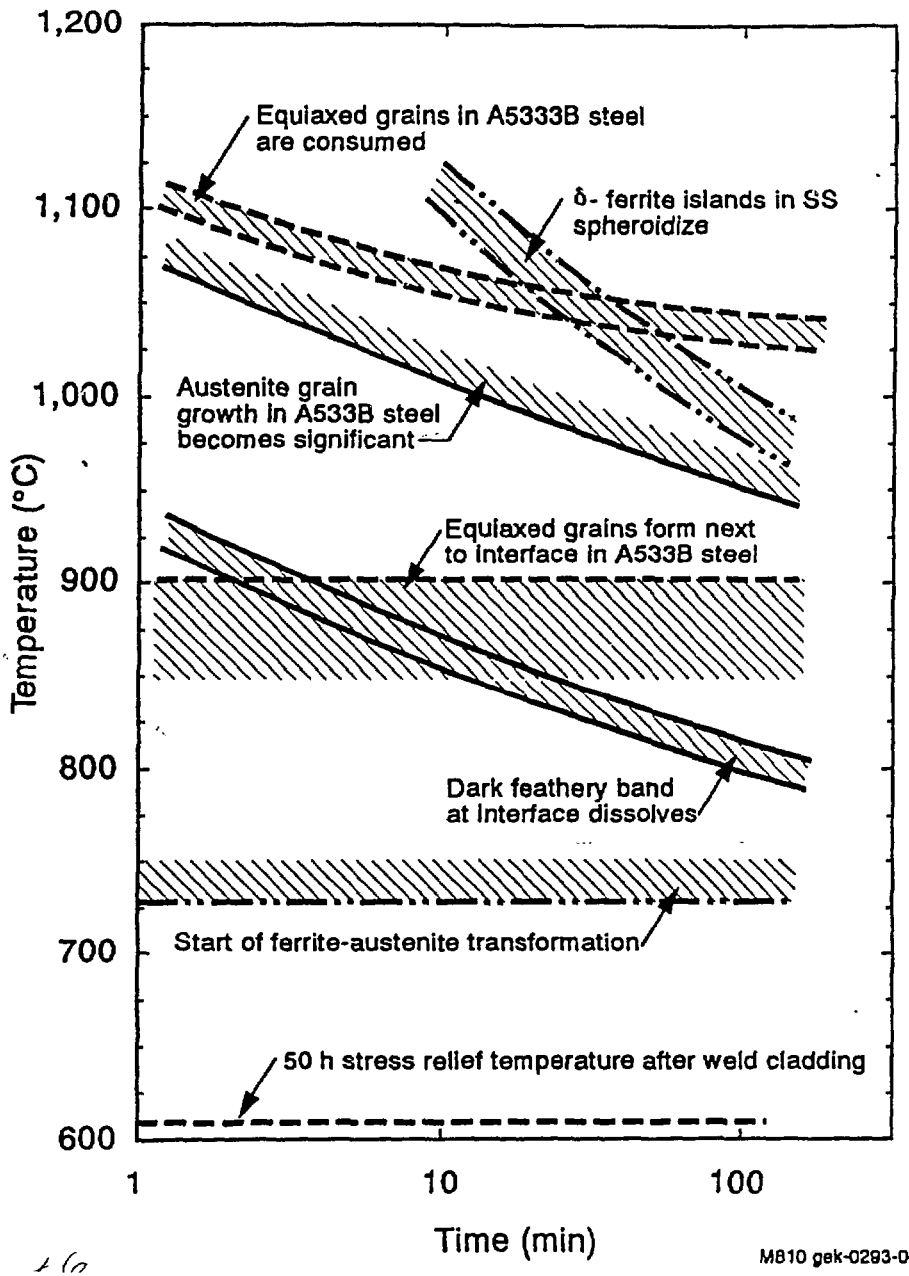

Fig. 6. Diagram of time-temperature observations of A533, Gr. B pressure vessel steel clad with Type 308L stainless steel.

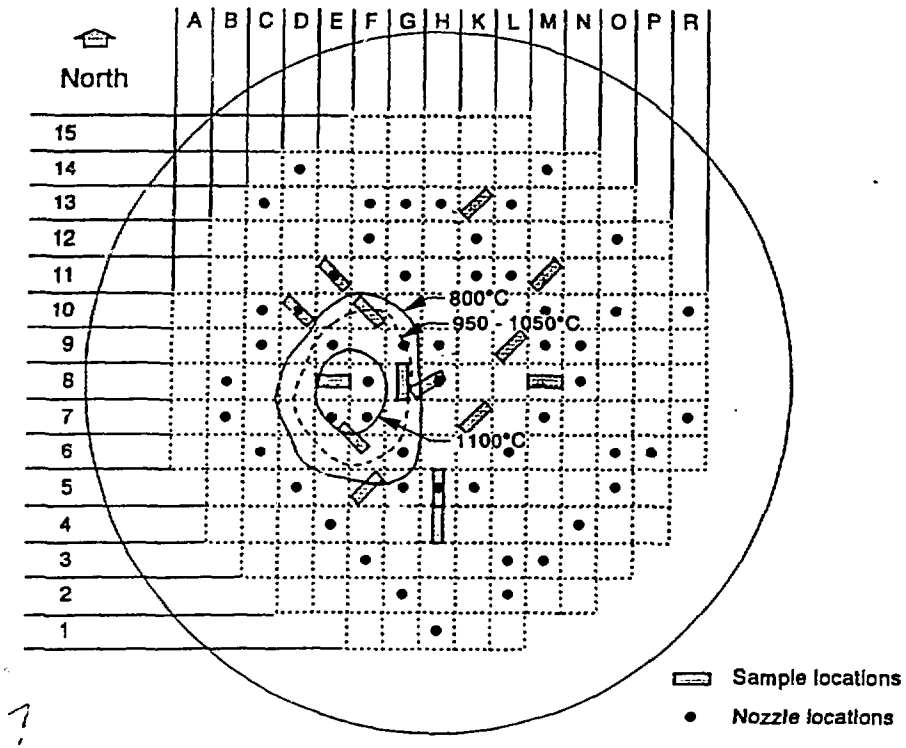

Fig. 7. Thermal contour map of peak temperature constructed as best estimate based on results of the metallographic examinations of the boat samples.

metallurgical examinations (INEL) estimated peak temperatures and time at temperature within ≈2.5 mm of the weld clad/base metal interface as follows:

- E-6 and E-8: 1075-1100°C for about 30 minutes
- F-10 and G-8: 1040-1060°C for about 30 minutes.

Examinations at ANL and some of the OECD partner laboratories for different sections of these same boat samples are consistent with the INEL conclusions. United Kingdom researchers showed evidence that M-11 also slightly exceeded the 727°C transformation temperature, but that determination was not confirmed by the other five laboratories examining different sections of the M-11 boat sample. Based on the above observations and conclusions, a thermal contour map of peak temperatures was constructed as shown in Fig. 7. The hardness profile and microstructure of one of the thermally altered samples, E-8, is shown in Fig. 8.

The temperature gradient through the thickness of the lower vessel head wall was estimated by two methods. First, since the high level of hardness of the four affected samples persisted to the full depth of the boat samples (50 mm from the inside surface or 45 mm

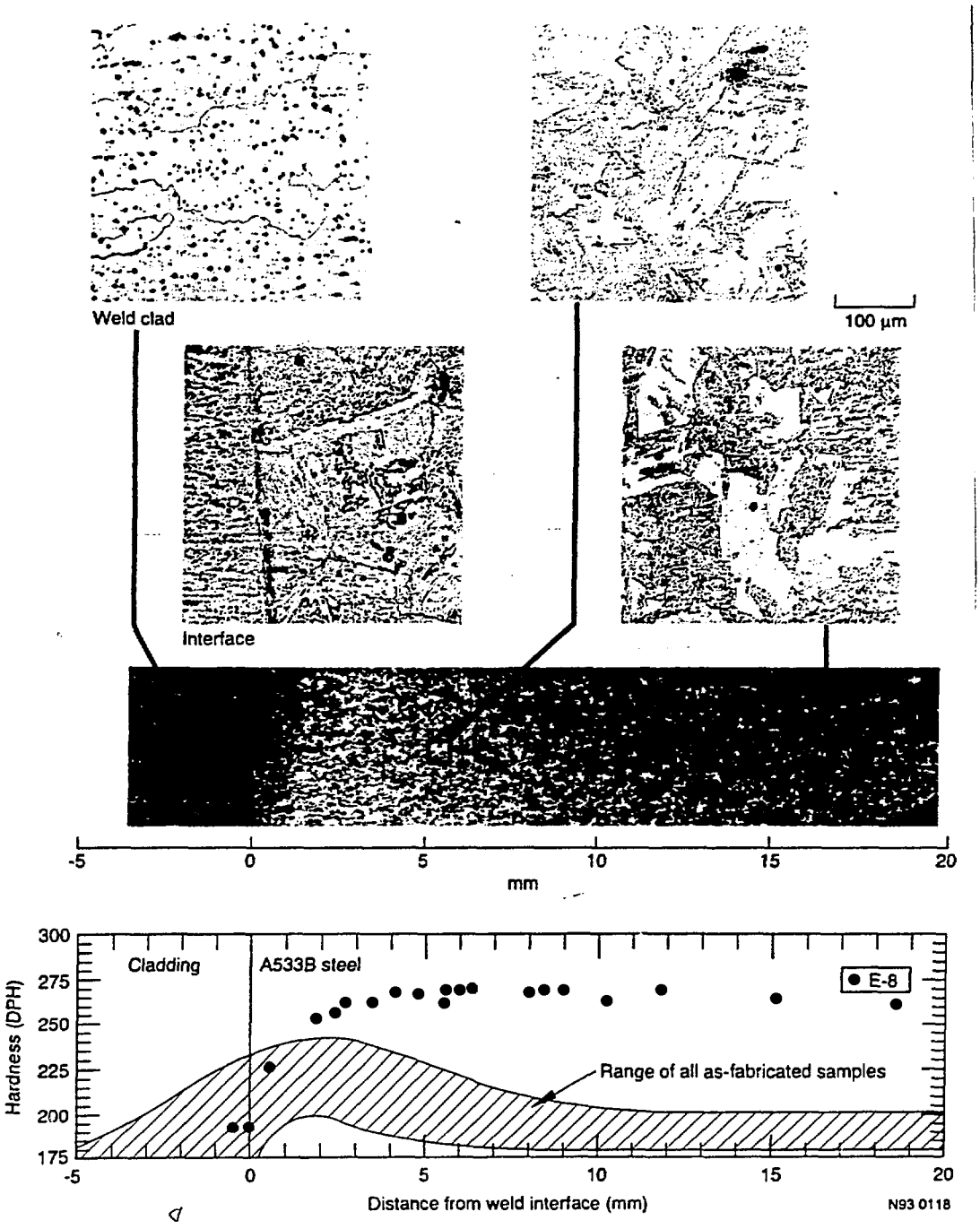

Fig. 8. Microstructure and hardness profile of Sample E-8.

Fig. 9. Cross section through principal crack in Sample E–6.

from the weld clad interface; see Fig. 5), it could be concluded that the temperature at that depth was greater than the 727°C transformation temperature. Secondly, based on the assumption from the microstructure comparisons that the thermal excursion on the lower head due to the accident was on the order of 30 minutes, prior austenite grain size at the bottom-most tip of the heat-affected samples was compared with the prepared standards given the 30-minute heat treatments. The results of this comparison indicated that the temperature 50 mm from the inside surface (45 mm from the stainless steel/low alloy steel interface) was approximately 50–150°C lower than the peak temperatures determined previously for the region near the interface. By combining all the temperature gradient estimates from INEL, ANL, and Finland, and assuming a linear relationship, the gradient appeared to be 2-4°C/mm.

Examination of Cladding Cracks. Results of the metallographic examinations through the cracks in samples E-6 and G–8 indicated that the cracking originated in and was essentially limited to the Type 308L stainless steel cladding used on the vessel. A cross section through the principal crack in E–6 is shown in Fig. 9. Penetration into the A533 vessel steel was only superficial (≈3 mm). This was also the case for the two cracks examined from the G–8 sample, where the maximum penetration was somewhat greater (≈6 mm).

The rent nature of the 308L stainless steel within the crack of E-6, which was also typical of the G-8 crack, is evidence of the elevated-temperature ductility of the Type 308L weldment and the hot tearing along interdendritic boundaries that resulted in the cracks. The hot tearing would have been caused by the thermal stresses when this hot-spot area cooled rapidly at ≈10-100°C per min.

The SEM examination of the materials found in the E-6 and G-8 cracks revealed evidence of molten material that was present at, or shortly after, formation of the cracks. The principal constituents of this material, which appeared to be layered on the exposed crack surfaces, were Fe, Cr, and Ni, together with Sn, In, Ag, and Cd in combinations as second phases or discrete metallic particles within the general oxidized matrix. The appearance of the material indicated that it was not a surface oxidation product, but had once been molten and was interacting with the cladding in a solid/liquid reaction. These elements are the essential constituents of the Zircaloy-shrouded, stainless-steel-clad Ag-In-Cd control rods. The extensive gray structure in the root of the crack, however, was principally the Fe oxidation product of A533 vessel steel laced with a solidified Sn-In phase. Fuel particles were found only on top of the oxidized layers or as minor constituents of the layers. The absence of significant quantities of fuel in the cracks indicates that the massive fuel flow to the lower head was not the source of the solidified material in the cracks.

Inclusions of Ag-Cd were found in numerous intergranular tears on the surface and well into the cladding (≈4 mm), as shown in Fig. 10. It is quite likely that interdendritic penetration of these materials as liquids contributed to the hot tearing of the cladding. Copper was also found in the cladding, next to the cracks, suggesting another causative agent for the hot tearing.

These observations on the superposition of core materials in the cladding and in cladding cracks suggest that the control-assembly materials were already on the lower head when the massive fuel flow from the core region arrived. Because the control-assembly materials would have reached the lower head as solids, they apparently were remelted by the fuel flow, resulting in intergranular penetration of the cladding by Ag-Cd.

Examination of Instrument Tube Nozzles

Background Information. Fourteen instrument-tube-nozzle segments were removed from the lower head of the TMI-2 reactor for detailed examinations as part of the Vessel Integrity Project (VIP). Six of these were examined at Argonne National Laboratory-Illinois (ANL) and eight were to be examined at the Idaho National Engineering Laboratory (INEL). The objectives of the nozzle examinations at ANL were to (1) provide information on the temporal and locational movement of fuel onto and across the lower head; (2) estimate peak temperatures of the nozzles from their metallurgical end-state; and (3) determine the mechanisms, modes, and extent of nozzle degradation to evaluate the possible damage to the lower head. Corollary objectives to focus the examinations were to (1) determine the nature and extent (axial and radial) of fuel/debris ingress into a nozzle; (2) determine the nature and degree of chemical and thermal interaction between fuel, debris, and nozzles; (3) determine thermal-related metallurgical changes in the nozzles as a function of axial position to evaluate the axial temperature distribution and attempt to quantify temperatures near the vessel; and (4) determine the position and composition of debris adhering to nozzle surfaces to establish a "debris bed depth." Because of problems with the hot-cell, the examinations at INEL were

Fig. 10. Inclusions of Ag-Cd in intergranular tears in cladding of Sample G-8.

not as complete as planned. Therefore, the results presented in this paper will be principally from the ANL examinations.

The nozzle segments received at ANL were from locations D-10, E-11, H-5, H-8, L-6, and M-9 (Fig. 1). These nozzles exhibited the range of damage suffered by all the nozzles, i.e., from melt-off at a low elevation to none, and, based on their core location and degrees of damage, were representative of those at INEL, also.

The detailed results of these nozzle examinations are reported in Ref. 13. Only the most significant findings are summarized in this paper.

Examination Methods. The examination methods used at ANL consisted of visual examination and macrophotography, axial gamma scanning for ^{137}Cs, macroexamination of cut surfaces, metallography, microhardness measurements, and scanning electron microscopy/energy-dispersive X-ray (SEM-EDX) analysis.

The nozzle segments were systematically sampled for detailed examination to obtain the desired data. Sectioned areas were based on the following attributes: (1) top and bottom locations, to obtain information on the hottest (sometimes molten) and coldest (nearest the vessel) temperature extremes in a nozzle; (2) fuel/nozzle interaction areas (nozzle degradation

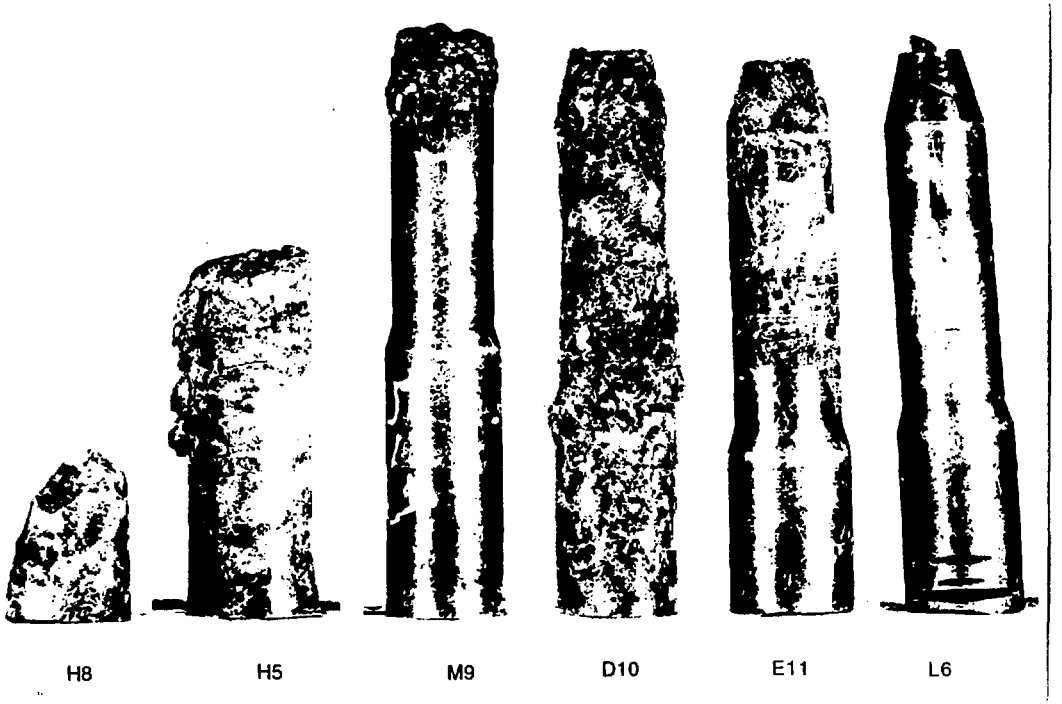

Fig. 11. Appearance of nozzles as removed from the lower head.

mechanism); (3) indications from gamma scans of fuel penetration into the nozzle; (4) obvious locations of debris on a nozzle; and (5) locations of surface cracking (nozzle degradation mechanism).

Pattern of Nozzle Damage. Figure 11 shows the as-removed appearance of the six ANL nozzles; Table 1 should be used to obtain a true comparison of the elevations at which nozzle damage occurred because the stub lengths remaining on the vessel were different for each nozzle. The tops of nozzles M-9 and H-5 were clearly melted an appreciable amount. The transition zone between the molten region and the unaffected lower part of the nozzles was relatively narrow on M-9 and more extensive on the shorter H-5. These transition zones were typically covered with a thin scale that was basically an iron oxide with entrapped shards of various core debris materials (Fig. 12); the lower areas of the nozzles were clean of adherent scale and showed little, if any, effects of being in contact with very hot core debris.

Significant fuel penetration into these molten nozzles was essentially limited to the melted and scaled elevations, i.e., the hot top of the nozzle. The material found in the top of nozzle M-9 (Fig. 13) was a mixture of solidified fuel and nozzle remnants in a matrix of chromium oxide from the Inconel 600 nozzle material; this oxide was different from the Fe-based oxide scale on the outside of the nozzles. It is believed that the ability of the fuel to penetrate downward into the nozzle was limited by the Cr oxide in which it was trapped (Cr_2O_3 melts at 1990°C).

Table 1. ANL Nozzle Segment Lengths, Elevations, and Fuel Penetration Depths (in mm)

Nozzle	Elevation of Nozzle Base[a]	Segment Length	Stub Length	Elevation of Top of Segment[b]	Fuel Penetration Elevation above Nozzle Base[c]	Condition
M-9	119	254	26[d]	280	241	Melted off; some scale
L-6	94	241	634[d]	305	75	Intact, shiny
H-5	107	146	0	146	89 max 117 min	Melted off; scale
H-8	0	70	51	121	<64	Melted off; liquid ablation in center
D-10	244	235	57[d]	292	55 max 184 min	Crusted and softened one side
E-11	221	225	77[d]	302	204	Tip melted; scale

[a]Referenced to vessel low point at H-8.

[b]Referenced to nozzle base.

[c]Based only on gamma scans.

[d]Calculations as the difference between 305 mm and the sum of the two known values. Measurements of stub lengths for D-10 and E-11 from photographs were not deemed sufficiently accurate because of angle of photo.

Fig. 12. Layer of Debris on Outer Surface of D-10 at the 82-mm Elevation. (190X, 281852)

Fig. 13. Longitudinal Section through Top of Nozzle M-9 (7X).

The H-8 nozzle segment received at ANL was only the bottom portion of a longer post-accident segment, the top of which was broken off during the removal operations. The top surface of the bottom portion, shown in Fig. 11, was smooth compared to the melted regions of M-9 and H-5. Upon detailed examination by SEM-EDX, it was found that this surface had reacted extensively with a molten Zr-rich phase that contained ingots of Ag-Cd. These elements would have come from control assembly components that apparently melted early in the accident and deposited on the lower head in advance of the major fuel flow there. Intergranular penetration of Ag-Cd was found in a number of nozzles and into the surface of the vessel cladding.[3]

In contrast to the melted condition of nozzles M-9 and H-5, nozzle L-6 (almost midway between them on the lower head) showed no external damage at all. This indicates that the fuel movement in the lower head was not one unified flow, but rather individual flows from different directions.

Although the surface of nozzle L-6 was clean, the nozzle contained solidified fuel masses down to within 75 mm of its base, the deepest penetration in any nozzle. This deep penetration is attributed to the lack of fuel/nozzle interaction that would have formed a binding Cr oxide. Because both the nozzle and its overlapping guide tube were undamaged, the source of this fuel is not obvious: it would have been difficult for molten fuel to have come up under the guide tube and down into the nozzle without damaging either unless the fuel was not very hot but still mobile. It could be concluded that the fuel came down directly through the guide tube from somewhere up in the reactor.

Nozzle D-10 was at the periphery of the lower head and appears to have been on the edge of the flow of molten fuel. One side of the nozzle was heavily crusted along its entire height, while the other side, in a 180° arc, showed only the more common light surface scale. Upon sectioning, it was found that an unexplained internal pressurization had pushed out the hot, crusted side of the nozzle, making it egg-shaped in cross section. The internal pressure created a crack in the outer surface of the nozzle and also collapsed the inner Inconel 600 tube of the instrument string. The body of the nozzle had undergone intergranular hot tearing, which apparently penetrated to the surface and formed the crack. The nonuniform damage indicates that these events occurred quickly, with no time for heat transfer to the

rest of the nozzle. This could be expected at the edge of a fuel flow coming to rest against the nozzle.

The last nozzle, E-11, was damaged only at its tip, below which was a fairly extensive area of the Fe-based scale. Melting was limited to the inner and outer surfaces of the tip, with indications of rapid melting and solidification. Fuel penetration was relatively deep (compared to that in M-9) apparently because the temperature at the top was too low to form Cr oxide that likely would have limited downward fuel movement. Instead, the material in the tip of the nozzle was in an Fe-based oxide, similar to that of the surface scales.

Two principal points may be concluded from the variable degradation of the instrument tube nozzles. First, considering that most of the nozzles on the lower head were covered with a hard, solidified layer of fuel debris, but that nozzles such as L-6 sustained no outward damage from contacting this debris, it can be concluded much of this debris acted as an insulator and protector of both the nozzles and the lower head. The absence of virtually any indication of degradation in the bottom parts of nozzles (even in those whose tops had melted) indicates that what was likely the first fuel debris to reach the lower head solidified relatively quickly and built up a significantly thick insulating layer. Once this layer had built up, the later material arriving on top of the solidified material melted off the tops of those nozzles that were exposed. The elevations at which these melt-offs occurred provide evidence for the thickness of the initial protective layer at various locations around the lower head. Thus, the fact that the nozzles in the vessel hot-spot area of E-F/7-9 were melted down the most indicates that only an initially thin insulating layer existed there, which apparently was the reason the hot spot formed where it did.

The second point that may be concluded is that the fuel debris movement across the lower head was not one massive, unidirectional flow, but more likely a number of flows from different directions. This derives from the lower head locations where specific nozzles melted off and the elevations at which they melted. The melt-off of M-9, in the eastern side of the lower head at a relatively high elevation, indicates a thick initial layer there with the subsequent hot fuel moving downward toward the reactor center atop this thick crust. Similarly, nozzles H-5 and G-5 were melted off atop a somewhat thinner initial crust, whereas nozzle L-6 did not melt because it was totally covered initially with relatively cold debris. These crust thicknesses are likely indicative of the amount of molten core material that initially solidified on these locations, and indeed these locations correlate with the locations in the elliptical flow distributor through which debris is believed to have come. Debris flowing downward atop initial crusts at M-9 and H-5 would effectively be moving toward the area of short, melted-off nozzles where the vessel hot spot occurred.

Penetration of Materials into Nozzles. The penetration of gamma-active materials downward into the nozzles was estimated from the ^{137}Cs gamma activity profiles; the results are summarized in Table 1. It was assumed that the gamma activity was associated with fission products in fuel, and therefore the results are reported as "fuel penetration." Metallic debris, essentially molten Inconel from the nozzle, was also found in the nozzles, but not tabulated.

Although porous, ceramic-appearing material was seen in the as-cut transverse sections at elevations below the nozzle tops, such as in H-8 and L-6, there seemed to be difficulty in retaining this material during the subsequent sectioning operations to form metallographic mounts. This attests to the friable nature of the material. In most cases, fuel material that

was retained at the lower elevations had two features. First, it appeared to be in the early stages of transformation to U-rich and Zr-rich phases, indicating relatively rapid cooling. Second, it contained Fe, Al, and Cr in the grain boundaries, indicating likely fluidity significantly below 2000°C. That would aid the fuel's mobility to the elevation where it finally solidified.[14]

In nozzles M-9 and H-5, which melted off, the penetration was shallow; this indicates a quick melting and relatively rapid cooling, notwithstanding the phase transformations in the fuel areas. It is likely that the melting point of Cr oxide dominated the mobility of this material before thermal equilibrium and lower-melting eutectics could form. The phase transformation of the fuel would have occurred below 1990°C while the solidified fuel was trapped in the insulating Cr oxide. In contrast, porous fuel was found at the base of the H-8 nozzle segment, far below where the nozzle apparently had melted, i.e., in the part of the nozzle not received at ANL. This fuel may have entered the breach where the nozzle had interacted with liquid Zr and at too low a temperature to form Cr oxide.

The fuel in the tops of D-10 and E-11 differed from that in M-9 and H-5 in that it was trapped in an Fe- rather than a Cr-based matrix. This reflects two probabilities. First, the Inconel did not readily give up its Cr to oxidation, probably because the temperature was too low. Second, the source of the fuel and the Fe-based matrix was probably the same as that of the Fe-based surface scales. That many of the fuel particles were shards and not solidified in-situ masses indicates that the fuel flow in this region of the vessel was cooler than the flow that contacted M-9, H-5, and H-8. This is consistent with a scenario that has the fuel flow coming to the vessel hot spot from the east and south and piling up on the far side against D-10 and E-11. (Note that the surface crust and major heating load was only on one side of D-10.)

Presence of Control Assembly Materials. There is pervasive evidence from the ANL examinations that materials from assemblies containing Ag-In-Cd deposited in some form, probably as solid particulates, on the lower head before the principal fuel flow occurred at 226 minutes. Unfortunately, there is no direct, unequivocal evidence that a control rod debris bed existed on the lower head. Most, if not all, of such a control rod debris bed would have remelted and possibly been consumed when it came in contact with even the initial, cooler fuel that reached the lower head first. Therefore, evidence for such a bed would now be, at best, on a microscopic scale and fortuitously derived.

The evidence that exists incudes the following: (1) the finding of Ag-Cd nodules and In-Fe-Ni-Zr phases solidified the vessel cladding cracks of boat samples E-6 and G-8; (2) significantly higher than expected Zr and Ag-Cd content on surface of H-8 nozzle; (3) Ag and Ag-Cd penetrating intergranularly into the surface of numerous nozzles, and (4) a layer of 10-μm, Ag-Cd particles on the surface of E-11, beneath the fuel debris scale.

The significance of a control material debris bed could be twofold. First, intergranular penetration of the vessel cladding by Ag-Cd may have played a role in the hot tearing of the cladding. And second, control material interaction with the nozzle material was at a low elevation that may have allowed greater penetration of molten fuel into nozzle H-8 than otherwise would have occurred. A third consideration, a potential insulating effect of the debris bed on the thermal impact to the vessel, could not be supported by a heat transfer analysis.

Mechanical Properties Tests

Test specimens were cut from the lower head samples in order to determine the mechanical properties of this material under the accident conditions. The tests conducted included tensile tests at room temperature and 600-1200°C, stress-rupture tests at 600-1200°C, and impact tests over the temperature range from -20 to +300°C. The room temperature tensile tests were conducted for the purpose obtaining comparisons with literature data; the minimum temperature of 600°C for the remaining tests reflects the judgment that little or no damage would have occurred to those portions of the lower head for which the maximum temperature did not exceed this value and that failure was unlikely at these locations. The maximum temperature of 1200°C for these tests lies slightly above the maximum lower head temperature believed to have been attained during the accident.

The tests were conducted on specimens with various prior thermal histories resulting from the accident. Because the number of specimens from the highest-temperature portion of the lower head was limited, it was necessary, in some cases, to heat treat low-damage specimens before testing to produce the corresponding microstructure. This heat treatment consisted of heating the specimen to 1000°C, holding it at this temperature for 2 h, and then cooling it to room temperature at ≈10-50°C per min. For specimens to be tested at 1000°C or greater, this prior heat treatment was omitted, because its effects would be negated by the thermal treatment imposed during testing.

Tensile Tests. The tensile tests were conducted in general accordance with ASTM Standards E8 and E8M, using a rectangular-cross-section specimen that also complied with applicable standards of the Deutsches Institut für Normung (DIN). All elevated-temperature tests were conducted in an Ar or He environment. The strain rate for the elastic portion of the loading was $\leq 5 \times 10^{-4}$ s^{-1}, and the strain rate during plastic loading was 4×10^{-4} s^{-1} $\pm 1 \times 10^{-4}$ s^{-1}. The reported yield strength values were obtained by the 0.2% offset method, except where discontinuous yielding occurred; in these cases, the observed upper yield strength was reported.

The results of the tensile tests conducted on the lower head base-metal specimens are presented in Fig. 14. These tests were carried out at ANL as well as in Belgium, France, and Spain. Also plotted in Fig. 14 are average values reported by the Japanese National Research Institute for Metals (NRIM) for five other heats of A533, Grade B steel.[15] The NRIM data were obtained at a strain rate of 5×10^{-5} s^{-1} up to yield and 1.25×10^{-3} s^{-1} for the remainder of the test. The NRIM tensile strength data suggest a strain-aging effect between 100 and 300°C, resulting in a local tensile strength minimum at ≈150°C. Both the tensile and yield strengths of this alloy are strongly temperature dependent; the room-temperature values are reduced by more than a factor of 2 at 600°C and by more than a factor of 10 at 900°C.

The data for specimens taken from lower head samples E-6 and E-8 are plotted separately in Fig. 14, and these data lie significantly above the best-fit curve to the remaining data. It has been determined that both of these samples were heated to maximum temperatures of ≈1000-1100°C during the accident, followed by a relatively rapidly cooling.[2] The resulting hardening has produced significant increases in strength at both room temperature and 600°C.

Stress-Rupture Tests. The stress-rupture tests used the same specimen design as the tensile tests, and testing was carried out in general accordance with ASTM Standard E139.

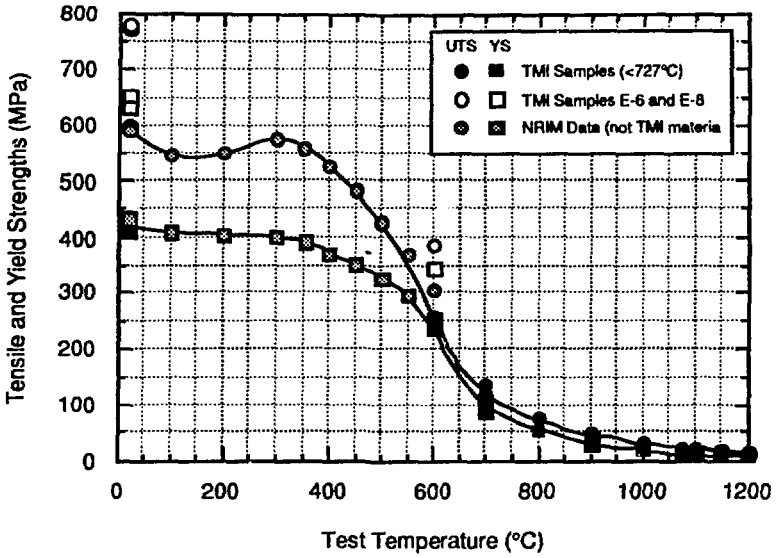

Fig. 14. Tensile and yield strengths of TMI-2 lower head material

These tests were carried out at ANL and in Belgium, France, and Spain, and the resulting stress-vs.-time-to-failure data are plotted in Fig. 15. The tests were conducted in an Ar or He environment except those conducted by the SCK/CEN in Belgium. All but one of the Belgian tests was conducted in vacuum; a single test at 800°C and 30 MPa was conducted in an Ar environment.

Materials with slightly different thermal histories were tested at both 600 and 700°C. At 600°C, tests were conducted on specimens from Sample K-13, for which the maximum temperature during the accident did not exceed 727°C, as well as on specimens from Sample F-5, for which the maximum temperature was apparently somewhat >727°C over a portion of the sample. No significant difference in time to failure is observed in Fig. 15. This lack of an effect may be attributed to the fact that the maximum temperature probably did not significantly exceed the transformation temperature of 727°C in F-5, particularly in the bottom half of the sample from which the creep test specimens were taken. Similarly at 700°C, specimens from Sample M-11, for which the maximum temperature may have approached or slightly exceeded 727°C, show no difference in behavior when compared with specimens from Sample H-8, for which the maximum temperature remained below 727°C.

Two time-temperature correlations were explored in an attempt to fit the base-metal creep data. The first of these was the Larson-Miller parameter L[16]

$$L = T[C + \log_{10}(t_f)],$$

where T is temperature in Kelvin, t_f is time to failure in hours, and C is a fitting constant. A least squares analysis determined that the optimum value of C for the present data base was 12.5, and stress s was related to the Larson-Miller parameter by the relation

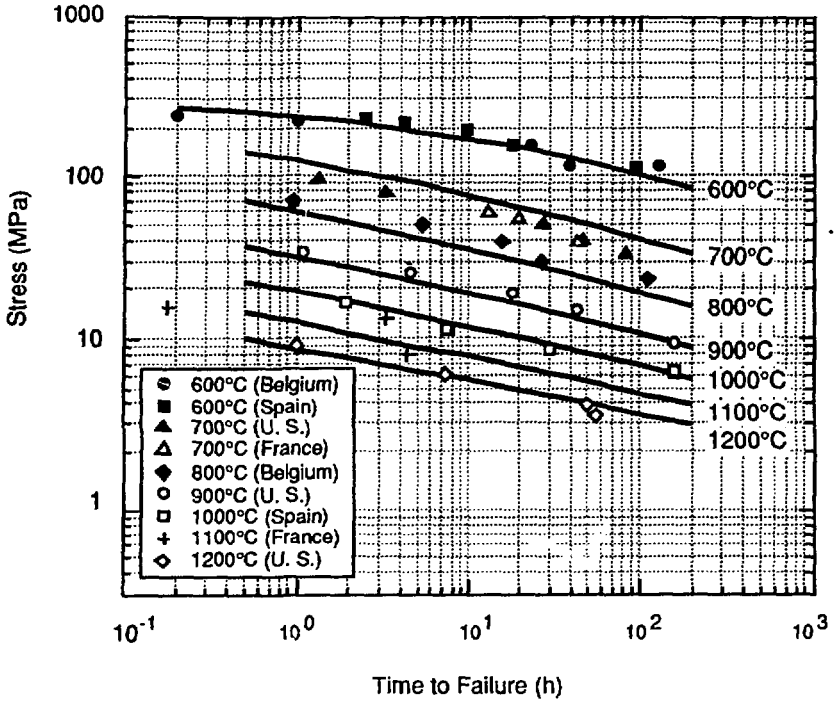

Fig. 15. Stress-rupture data with Manson-Haferd best fit

$$\log_{10}(s) = 4.3406 - 0.00018767 \cdot L, \qquad (1)$$

where the applied stress s is in MPa.

The ability of the Manson-Haferd time-temperature correlation[17] to the data was also evaluated. The Manson-Haferd parameter M has the form

$$M = \frac{\log_{10}(t_f) - t_a}{T - T_a},$$

where t_f is time to failure in h, T is test temperature in Kelvin, and t_a and T_a are fitting constants. A least squares analysis was again carried out, and the optimum values for t_a and T_a were found to be 7.57 and 520 respectively. Log(s) was found to vary with the Manson-Haferd parameter M according to the relationship

$$\log_{10}(s) = -0.80467 - 261.41 \cdot M - 5291.25 \cdot M^2. \qquad (2)$$

A comparison of the resulting best fit curves with the actual s vs. t_f data in Fig. 15 shows a reasonably good fit to the data. However, systematic departures from the actual data are noted in the 700-900°C region. This problem may be associated, in part, with the ferrite-to-austenite phase transformation that occurs over the temperature regime from 727 to ≈850°C.

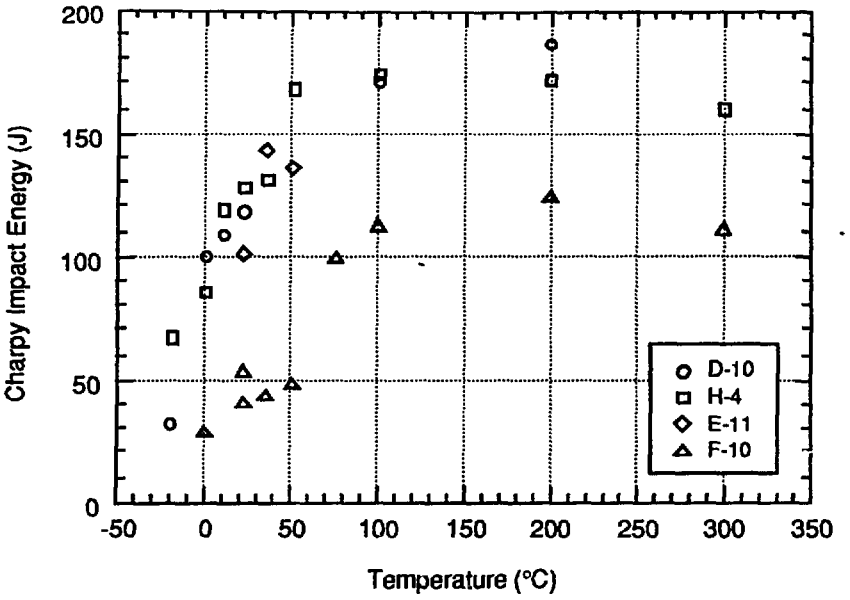

Fig. 16. Absorbed impact energy vs. test temperature

Impact Tests. The impact tests on the lower-head material were conducted in Italy[8] using the procedure and conventional Charpy V-notch test specimen described in ASTM E23, and the data are summarized in Fig. 16. The three groups of test specimens for which the maximum temperature did not exceed 727°C show similar behavior, with an upper shelf energy of ≈170 J and a transition temperature of the order of 20°C. However, the data from specimens of Sample F-10, for which the maximum temperature was as high as ≈1050°C, stand in marked contrast. The F-10 material shows a significantly higher ductile-to-brittle transition temperature of ≈70°C, as well as a lower upper-shelf energy of ≈120 J. These differences reflect the reduced ductility and impact resistance that is produced in this material by the high temperatures and relatively rapid cooling associated with the accident.

Summary and Conclusions

Microstructural characterizations and mechanical properties tests have been conducted by INEL, ANL and the OECD partner laboratories on material from 15 locations in the lower head of the pressure vessel of the TMI-2 nuclear reactor. Instrument nozzles and guide tubes from the lower head were also examined. The microstructural characterizations were conducted by conventional optical metallography, hardness measurements, scanning electron microscopy (SEM) on etched specimens and surface replicas, and analytical transmission electron microscopy on thin foils and carbon extraction replicas. The mechanical tests consisted of tensile tests at room temperature, tensile and creep tests at 600-1200°C, and Charpy impact tests at -20-300°C. The specimens tested were taken from locations where the maximum temperature had not exceeded 727°C during the accident and from locations where the maximum temperature had been as high as 1100°C. The results of these investigations lead to the following conclusions:

1. An elliptical shaped hot spot approximately 1 x 0.7 m on the inside surface of the lower pressure vessel head was heated to temperatures from ≈800 to 1100°C for approximately 30 minutes due to the relocated fuel debris.
2. The remainder of the lower head remained below 727°C, but some areas may have been close to this temperature.
3. The temperature gradient through the thickness of the vessel wall was of the order of 2 to 4°C/mm.
4. The thermal excursion of the lower head was "quenched," i.e., cooled at a rate of the order of 10-100°C/minute.
5. The results of tensile tests conducted on base-metal specimens for which the maximum temperature during the accident (T_{max}) did not exceed 727°C agree well with literature data for A533B steel and show a dramatic drop in strength at temperatures above 600°C.
6. Tensile specimens from samples for which T_{max} exceeded 727°C showed significantly higher strengths at room temperature and 600°C when compared to specimens for which the temperature did not exceed 727°C.
7. Creep tests at 600 and 700°C indicated no significant difference in behavior between base-metal specimens for which T_{max} was of the order of 727°C and those for which it was well below this value.
8. The stress-rupture data obtained from base-metal specimens could be more accurately fit with a Manson-Haferd time-temperature parameter than a Larson-Miller parameter.
9. Charpy V-notch impact tests conducted on lower head base-metal material noted a substantial difference between specimens from Sample F-10, for which T_{max} was as high as ≈1050°C, as compared with specimens from samples for which T_{max} was <727°C. The F-10 material showed a significantly higher ductile-to-brittle transition temperature as well as a lower upper-shelf energy value.
10. Cracks through the stainless steel cladding of Samples E-6 and G-8 appear to have been hot tearing phenomena, probably assisted by interdendritic penetration of liquid Ag-Cd.
11. Materials in the cladding cracks suggest the presence of control-assembly debris on the lower head before the massive flow of fuel arrived.
12. The nature of the degradation of nozzles M-9, H-5, and H-8 indicate that their melt-off was by liquid fuel approaching the nozzles at elevations of ≈140 to 270 mm above the lower head. Surface scale on the nozzles below the melt-offs suggests that the liquid was atop a crust of solidified and partially solidified debris that had been cooled below its solidus by contact with the lower head.
13. The flow of very hot material on the lower head followed multiple paths. The damage to nozzles M-9, H-5, and H-8 suggests that flows occurred from the east and south, but apparently did not affect nozzle L-6 because it had already been covered by cooler material that had reached the lower head first. The pattern of nozzle degradation and the assumed fuel-flow directions are consistent with a vessel hot spot at E-F/7-8 where there was apparently only a thin protective crust.
14. The presence of significant quantities of Zr and Ag-Cd on the vessel to interact with the nozzles is attributed to the prior deposition at that location of control assembly material.

The depth or nature of such a debris bed could not be confirmed, but the depth is estimated to have been at least 120 mm at the H-8 location.

15. Fuel debris penetration downward into the nozzles was influenced by the temperature of the fuel at the time of entry; by the composition, and hence the fluidity, of the fuel; by the temperature of the nozzle and its ability to solidify the debris; and the degree of interaction between the fuel and the molten nozzle in entrapping the fuel in Cr oxide.

Acknowledgment

The authors gratefully acknowledge the support and direction provided for this work by C. Z. Serpan, E. Hackett, A. Rubin, and M. Mayfield of the NRC. The financial support and significant technical contributions made by the OECD partner laboratories participating in the TMI-2 Vessel Investigation Project Metallurgical Program are also gratefully acknowledged. The following persons at ANL contributed to the completion of this work: T. L. Shearer, D. O. Pushis, F. M. Basso, S. L. Phillips, J. A. Zic, W. Kettman, F. Pausche, J. E. Sanecki, A. G. Hins, W. F. Burke, and W. A. Moll. INEL contributors include G. L. Fletcher and D. V. Miley.

References

1. J. R. Wolf, J. L. Rempe, L. A. Stickler, D. W. Akers, G. E. Korth, L. A. Neimark, and D. R. Diercks, *OECD-NEA-TMI-2 Vessel Investigation Project Integration Report*, Idaho National Engineering Laboratory, TMI V(93) EG10, October 1993.

2. G. E. Korth, *Metallographic and Hardness Examinations of TMI-2 Pressure Vessel Samples*, TMI V(92) EG01, Idaho National Engineering Laboratory, January 1992.

3. D. R. Diercks and L. A. Neimark, *Results of Mechanical Tests and Supplementary Metallographic Examinations of the TMI-2 Lower Head Samples*, Argonne National Laboratory, TMI V(93) AL02, June 1993.

4. W. Vandermeulen and W. Hendrix, *Examination Report of the Samples of the TMI-2 RPV Received by SCK/CEN (Belgium)*, SCK/CEN, Mol, March 1992.

5. Reijo Pelli, *Metallographic Examination of TMI-2 RPV Lower Head Sample E-8 and the Archive Material of Midland Reactor*, TMI V(92) SF01, VTT Technical Research Centre of Finland, Espoo, April 1992.

6. F. Le Naour, *CEA Contribution to the TMI-2 Vessel Material Investigation Project*, N.T. SRMA 92-1956, Centre d'Etudes de Saclay, May 1992.

7. H. Ruoff, K.-H. Katerbau, and D. Sturm, *Metallographic Examination of TMI-2 Lower Pressure Vessel Head Samples*, TMI V(91) D001, Staatliche Materialprüfungsanstalt, Stuttgart, September 1991.

8. P. P. Milella and F. Bigagli, *Charpy V Testing of Specimens of the TMI-2 Vessel Lower Head*, TMI V(92) I01, ENEA, Rome, May 1992.

9. L. Pedrero and P. Veron, *Metallographic Investigation of TMI-2 Lower Pressure Vessel Head Samples*, TMI V(92) E002, Equipos Nucleares S. A., Mallaño, April 1992.

10. A. Ballesteros, *TMI-2 Vessel Investigation Project Creep Tests*, TMI V(92) E004, TECNATOM, Madrid, February 1992.

11. E. López Rincón, *Testing of Lower Head Specimens in Spain (Tensile Results)*, TMI V(92) E001, CIAT, Madrid, May 1992.

12. J. M. Titchmarsh and R. Cooke, *AEA-Technology Examinations of TMI-VIP Lower Head Samples*, TMI V(91) UK2, AEA Technology, Harwell, September 1991.

13. L. A. Neimark, T. L. Shearer, A. Purohit, and A. G. Hins, *TMI-2 Instrument Nozzle Examinations at Argonne National Laboratory*, TMIV(93)AL01, Argonne National Laboratory, February 1993.

14. R. V. Strain, L. A. Neimark, and J. E. Sanecki, Nucl. Technol. **87**, No. 1 (August 1989), pp. 187-190.

15. *Data Sheets on the Elevated-Temperature Properties of 1.3 Mn-0.5 M0-0.5 Ni Steel Plates for Boilers and Other Pressure Vessels (SBV 2)*, NRIM Creep Data Sheet No. 18B, National Research Institute for Metals, Tokyo (1987).

16. F. R. Larson and J. Miller, Trans. ASME, vol. 74, pp. 765-771 (1952).

17. S.S. Manson, "Design Considerations for Long Life at Elevated Temperatures," Proc. Int. Conf. on Creep, London, Oct. 3, 1963, pp. 1-27.